Surface & Coatings Technology 421 (2021) 127366

Contents lists available at ScienceDirect

Surface & Coatings Technology

journal homepage: www.elsevier.com/locate/surfcoat

Deposition of bioactive gelatin coatings on porous titanium: Influence of processing parameters, size and pore morphology

Y. Torres [a,*], B. Begines [b,*], A.M. Beltrán [a], A.R. Boccaccini [c]

[a] Departamento de Ingeniería y Ciencia de los Materiales y del Transporte, Escuela Politécnica Superior, Universidad de Sevilla, Seville, Spain
[b] Departamento de Química Orgánica y Farmacéutica, Facultad de Farmacia, Universidad de Sevilla, Seville, Spain
[c] Institute of Biomaterials, Department of Materials Science and Engineering, University of Erlangen-Nuremberg, Cauerstraße 6, 91058 Erlangen, Germany

ARTICLE INFO

Keywords:
Biphasic implant
Osteochondral defects
Porous titanium substrates
Gelatin coating
Structural characterization
Tribomechanical behavior

ABSTRACT

In this work porous commercially pure Ti substrates fabricated by spacer-holder technique (50 vol% NH_4HCO_3 and three range pores sizes, 100–200 μm, 250–355 μm and 355–500 μm) were coated with two types of gelatinous materials, one as a linear polymer (non-crosslinked) and another one crosslinked. The role of the crosslink, as well as the morphology, size and degree of interconnectivity of gelatins coatings on their tribo-mechanical behavior (*P-h* curves and scratch tests) were analyzed. Results revealed a new promising route to manufacture composite porous implants which are potential candidates to develop new treatments, not only for osteochondral defects, but also for other types of damages involving tissues of different nature (hard and soft) perfectly joined.

1. Introduction

Bone is a dynamic organ. It maintains itself by a continuous process of regeneration in which the action of osteoblasts and osteoclast are carefully balanced to conserve the bone mass [1]. However, this balance tends towards osteoclast activity with age after 40 years of age an important reduction of the bone mass and therefore density of the bone occur, which leads to fractures and degenerative illness such as osteoporosis [2–4]. In fact, the degradation of bone tissue and the derived pathologies are important diseases affecting the world population nowadays and are considered as a significant public health problem [5,6]. Quite often, the density and thickness reduction of the cortical bone comes accompanied by degradation of the articular cartilage. The combination of these two conditions leads to osteochondral defects, that could even induce the appearance of osteoarthritis and eventually disabilities [7]. Although some treatments such as autograft or allograft transfers or bioengineered tissue implantation are applied to address osteochondral defects, these are focused on the recovery of the articular cartilage only [8]. A convenient procedure to treat this disease is the use of biphasic constructs [9], also known as osteochondral implants, that could simultaneously remedy the defects in both bone and cartilage tissues. They consist in a rigid scaffold that replace the bone tissue and a flexible coating that mimics the cartilage. Indeed, Schaefer et al. [10] suggested that this type of implants is even recommended for chondral defects, in which the cortical bone is not affected, because they improve the implant integration since the cartilage-to-cartilage interface presents higher difficulty to merge than the bone-to-bone interface.

Currently, different biphasic implants have been already investigated. Some of them use polymeric materials as the subchondral phase. Thus, for instance, two kinds of hybrid scaffolds were developed by Swieszkowski et al. [11], both based on polycaprolactone (PCL). The first biphasic scaffold was composed of fibrin as the cartilage phase and porous PCL as the subchondral phase. The second system consisted of PCL, to promote cartilage regeneration, while a composite of PCL and calcium triphosphate acted as bone substitute. Other approaches involved proactive glass scaffolds for the subchondral bone part and for the cartilage layer [12]. However, the use of metals as bone replacement has also been widely investigated, specially Ti and its alloys due to their great biocompatibility, mechanical performance and superior corrosion resistance [13–15]. Metal implants could provide the biomechanical support required by the cartilage in the hydrostatic compression. In this sense, Frosch et al. [16] applied a fully dense Ti implant seeded by mesenchymal stem cells to achieve the regeneration of the hyaline-like cartilage. However, fully dense Ti implants present limitations such as a high Young's modulus, compared to bone, which causes the stress-shielding phenomenon [17]. To minimize this limitation, the use of

* Corresponding authors.
E-mail addresses: ytorres@us.es (Y. Torres), bbegines@us.es (B. Begines).

https://doi.org/10.1016/j.surfcoat.2021.127366
Received 28 March 2021; Received in revised form 10 May 2021; Accepted 25 May 2021
Available online 29 May 2021

porous Ti has been reported in the literature, regarding scaffolds made by manufacturing, powder metallurgy or foaming techniques [18–21]. Among the different technologies to fabricate porous Ti implants, the space-holder technique, based on powder metallurgy, stands out considering its versatility, reliability, and low cost [22–26], what points it out as the ideal technique to modulate the implant stiffness.

As previously mentioned, a biphasic implant is also composed of a flexible material that should mimic the cartilage tissue promoting its recovery. A broad range of materials, composites and scaffold has been tested for cartilage regeneration [7,9,27–29]. However, to our knowledge, the only research work proposing a biphasic implant based on Ti was carried out by Duan et al. [8]. In it, they presented an implant where the bone tissue was substituted by porous Ti while type I collagen dopped with glycosaminoglycan was used to mimic cartilage tissue. Although they demonstrated that this type of biphasic systems had very promising results for repairing osteochondral defects from a tissue regeneration point of view, in depth studies about the mechanical properties of the final implant are required to confirm their potential application *in vivo* and their long-term stability.

The main goal of this research work has been to manufacture and characterize a biphasic implant capable of solving both the stress shielding problems of titanium implants, as well as the possibility of replacing damaged soft tissue (osteochondral defects in cartilage). For instance, they could be used as potential solution for simultaneous replacement of damaged areas of bone tissues (for example, a tumor) located in an area of a joint (covered with cartilaginous tissues and replaced, in this case, by the gelatinous material). Gelatins are commonly used in tissue engineering for the regeneration of skin [30–32], cartilage [33–35] and bone [36–38]. Gelatin is a biopolymer obtained from the hydrolysis of collagen, the main constituent of connective tissues and bones of vertebrate animals [28]. In addition to its availability and biocompatibility, gelatin offers the possibility of modulation of its mechanical properties using its crosslinking capability when the right chemical reactions are applied. Therefore, in this work, it is proposed to evaluate the influence of porosity and the presence of crosslinks of porous gelatin obtained by the freeze-drying method on its tribo-mechanical behavior.

2. Experimental section

Porous titanium substrates were manufactured by the space-holder technique (SH) from commercially pure Ti (c.p. Ti) powder, grade IV [39], provided by SEJONG Materials Co. Ltd. (Seoul, Korea), with a mean particle size of $d_{[50]} = 23.3$ μm [40] and 50 vol% ammonium bicarbonate (NH_4HCO_3), (BA), provided by Cymit Química S.L. (Spain), which were sieved to separate them in different particle size ranges (100–200 μm, 250–355 μm and 355–500 μm). As depicted in Fig. 1 and according to the SH technique, c.p. Ti was mixed with the BA spacer particles for 40 min, to ensure the homogeneity of the mixture. The homogeneous blend was pressed at 800 MPa with an Instron 5505 universal testing machine (Instron, U.K.). The BA was later vacuum removed in an oven applying 60 °C for 10 h followed by 110 °C for another 10 h, at low vacuum (10^{-2} mbar). Finally, a sintering process (1250 °C for 2 h at high vacuum, 10^{-5} mbar) in a ceramic tubular furnace was applied to obtain the bare porous Ti samples.

The porosity of the substrates was studied by Archimedes' method for the determination of the density, total and interconnected porosity (ρ, P_T, and P_i, respectively) [41] . Also, the substrates were analyzed by image analysis (IA) by the measure of the equivalent diameter (D_{eq}) and the shape factor (F_f), defined by Eq. (1):

$$F_f = \frac{4\pi A}{(PE)^2} \tag{1}$$

where A is the pore area and PE is the experimental perimeter of the pseudo-elliptic pores.

Following, two different gelatin-based coverings were evaluated: the first one consisted of a coating prepared from gelatin from porcine skin, type A (powder, Sigma-Aldrich); the second one was a crosslinked version of the same gelatin. To prepare the coverings, gelatin was dissolved in deionized water (3% w/v) at 60 °C (Fig. 1). For the crosslinked material, a 7% (v/v) of a glutaraldehyde (Sigma-Aldrich) solution in deionized water (0.25 v/v) was added to the previous solution. Once the mixture was completely dissolved and turned homogeneous, it was poured into a well of a 24-well plate where a sample was previously deposited. After 12 h drying at ambient conditions, substrates were subjected to freeze-drying.

Gelatins were microstructurally characterized by Archimedes'

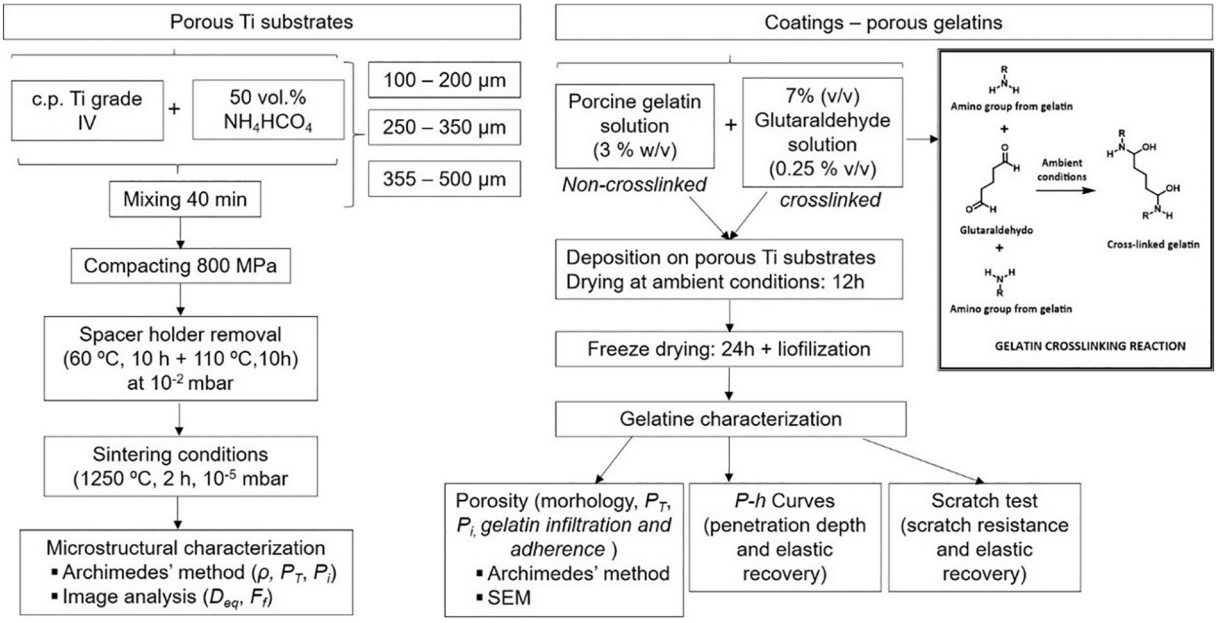

Fig. 1. Schematic of the complete manufacturing and characterization processes of coated porous Ti substrates. Note: the crosslinking reaction of the gelatin with glutaraldehyde is also included.

method (ρ, P_T, and P_i), carefully cutting small cubes of approximately 27 mm^3, and by SEM observations (size and morphology of the pores), although in this case just the top view of the gelatins was analyzed. On the other hand, the degree of gelatin infiltration and adherence to the porous titanium disc were investigated. To do so, gelatin was carefully removed from the titanium substrates to be able to observe the surface of the substrates. Then, SEM top-view images were acquired to evaluate the presence of remains adhered gelatin to the flat areas of the substrates as well as inside the pores.

Finally, the tribo-mechanical characterization of gelatin coatings was performed for the two types of gelatin, non-crosslinked and crosslinked. Since gelatin samples were not perfect cylinders and neither the top view was not completely flat, the surface of the samples was prepared by carefully cutting a thin layer of the outer layer and/or carefully polishing it by hand, to avoid damage to the surface and at the same time obtain a flat surface that would allow us to correctly carry out the tribo-mechanical characterization (P-h curves and scratch test). Besides, such polishing of the samples avoided that the tip of the indenter was in contact with the wrong area, leading to erroneous results. Instrumented micro-indentation technique was used for micromechanical characterization (penetration depth and elastic recovery), while to evaluate the scratch resistance, scratch tests were implemented at constant load. Both types of tests were carried out in a Microtest machine (MTR3/50–50/NI) fabricated by Microtest, S.A. Static loading-unloading tests (*P-h* curves) were conducted using a Vickers indenter. To ensure the contact between the indenter and the gelatin surface (top view), a preload force of 0.1 N was applied. The load–displacement curves were obtained by applying a maximum load of 1 N, at 0.25 N/mm and a dwell time of 10 s. On the other hand, scratch tests at constant load (1 N) were performed employing an indenter of 200 μm radius Rockwell C diamond stylus. The scratch length was set at 4 mm and a strain rate of 0.5 mm/min. The normal load is continuously recorded during scratching. Sliding contact response was given in terms of scratch penetration-load curves. Also, the corresponding friction coefficient was computed through the normal and tangential force, both measured by a strain-gauge type dynamometer. Further, the real plastic deformation and elastic recovery were evaluated, once the *in-situ* scratch test has finished, then the groove was examined at speed of 0.5 mm/min, in reverse direction and without applied load.

3. Results and discussion

3.1. Microstructural characterization of the c.p. Ti porous substrates and gelatins

Initially, and prior to the substrate coating, bare as-fabricated c.p. Ti samples were characterized in terms of porosity. In this sense, P_T, P_i, D_{eq} and F_f were measured by image analysis and Archimedes' method (Table 1). A total porosity around 50% was estimated (ranging just between 51 and 52%), according to the amount of BA added during the fabrication procedure. Also, the density was similar for the different substrates (~2.2 g/cm^3). However, the interconnected porosity was higher for the smaller pore size distribution (100–200 μm) and the morphology of the pores was less regular (F_f decreased). These two issues reinforce the idea that a higher probability of particle coalescence appears when the sizes of the applied spacer-particle are smaller. In the literature, mathematical equations are reported to relate the microstructural parameters with the mechanical behavior of porous titanium substrates [42]. Also, it is widely accepted that although the size of the pores favors the vascularization of the implant and infiltration phenomena [43–46], it can also compromise the tribo-mechanical behavior of the implant or scaffold. In this context, titanium substrates with a pore size in the range between 250 μm and 355 μm could have an enhanced balance of bio-mechanical and bio-functional behavior.

Table 1
Microstructural characterization of porous titanium substrates.

Range pore size (μm)	Archimedes' method			Image analysis		
	ρ (g/cm^3)	P_T (%)	P_i (%)	P_T (%)	D_{eq} (μm)	F_f
100–200	2.21 ± 0.16	51.1 ± 3.6	50.4 ± 4.1	49.2 ± 1.3	116 ± 28	0.68 ± 0.03
250–355	2.15 ± 0.11	52.2 ± 2.4	49.2 ± 3.6	54.6 ± 1.8	240 ± 19	0.84 ± 0.01
355–500	2.22 ± 0.12	50.7 ± 2.6	45.2 ± 3.6	48.5 ± 1.2	403 ± 26	0.79 ± 0.02

As depicted in Fig. 2, the gelatin coatings were obtained as soft foams, of white colour in the case of the non-crosslinked covering, and yellowish in the crosslinked material. Once the coverings were obtained, their densities and porosities were characterized, both estimated by the Archimedes' method after cutting the coatings in small cubes with a knife (Fig. 3). The densities of all coatings were very similar, ranging from 0.032 to 0.037 g/cm^3. However, it is worth mentioning that, in the case of the non-crosslinked gelatin, the density values did not follow a trend, probably due to different polymer chain orientations when the sample was freeze-dried, mainly considering that for the non-crosslinked gelatin the polymeric chains could freely move in solution; for the crosslinked materials, a slight reduction in the density values was observed. Regarding the porosity, all samples showed a total porosity very close to 100%. For the non-crosslinked gelatin, the interconnected porosity was similar in all cases, however, for the crosslinked polymeric material, there was a clear increment in the interconnected porosity with the increase of the spacer sizes of the substrates, probably due to an increment in the water content, as the decrease in the density points out.

As previously mentioned, the combination of porous c.p. Ti substrates with gelatin-based coatings was proposed as a potential candidate to solve the stress shielding problems in cortical bone tissue and the osteochondral defects in articular cartilage. Once the reliability of the fabrication of the porous Ti substrates was demonstrated, the gelatin-based coating had to be evaluated. For this purpose, two types of coatings were suggested: one based on pure porcine gelatin, Type A, and another based on porcine gelatin crosslinked with glutaraldehyde, (Fig. 1). In both cases, a gelatin solution (3% w/v) was prepared in deionized water. However, for the crosslinked gelatin, a 7% v/v of a glutaraldehyde solution (0.25% v/v) in deionized water was added. The presence of the aldehyde groups of the glutaraldehyde leads to a Schiff's Base reaction with the pendant amino group on the lysine residues present in the proteinic chain. The reaction of the two-aldehyde groups in the same glutaraldehyde molecule with two different gelatin chains is translated into the crosslinking of the polymeric material [47].

SEM studies (Fig. 4) demonstrated that, in general terms, the pore size of the coatings increased with the spacer size of the substrates. In addition, the pore size distribution seemed more homogeneous for the crosslinked gelatin, which reinforced the idea of a random distribution of the proteinic chains in solution when the material was non-crosslinked, entailing a higher randomized generation of pores. However, the freedom of movement of the gelatin chains was drastically reduced with the crosslinking leading to a homogeneous distribution of the material. Besides, crosslinked gelatin generally replicated the porosity of the substrate onto which they were deposited. A reticulated structure was observed, like a honeycomb, with a preferential orientation. The size of the channels was estimated by the linear intercept method, revealing an average size of 135 ± 17 μm and 189 ± 29 μm, for the porous substrates 100–200 μm and 250–355 μm, respectively. This fact practically disappeared for the larger range pore size, which could be associated with the coalescence of the channels.

In addition, the proteinic coatings were perfectly fixed to the substrate surfaces. A good adhesion to the flat area of the c.p. porous Ti substrates was achieved. Moreover, a kind of anchorage of the gelatin to the wall of the pores was observed which enhanced the adhesion of the gelatin coating to the substrate. This fact was demonstrated by SEM

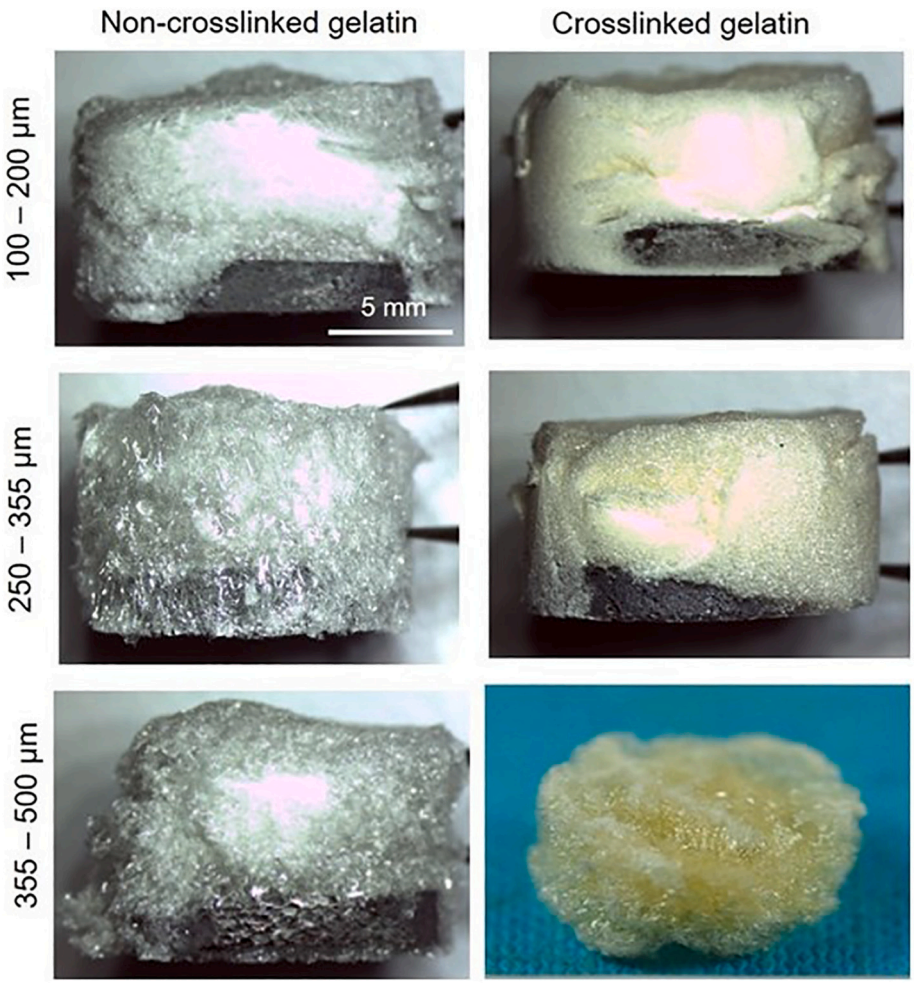

Fig. 2. Optical images of the bioactive gelatinous coatings. Common scale bar.

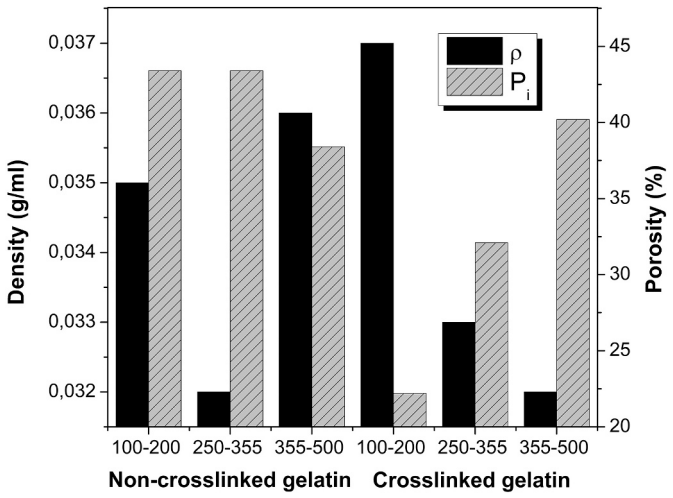

Fig. 3. Density and interconnected porosity estimated by the Archimedes' method in non-crosslinked and crosslinked gelatin samples. The total porosity was 99.5 ± 0.1% in all cases.

observations of the substrates' surface after cutting the coating at their interface level. Fig. 5 reveals that both gelatinous materials were able to enter and solidify inside the pores.

3.2. Tribo-mechanical characterization of the porous gelatin coatings

Concerning the tribo-mechanical behavior of the gelatin coated substrates, *P-h* curves and scratch tests were performed. It is worth to remark the role of the substrate in the tribomechanical behavior of gelatin. The tribomechanical tests were performed on the top-view of the gelatin coatings. The thickness of gelatin was large enough so the results were not influenced by the porous c.p. Ti substrate. Then, the effect of the substrate was negligible in measurements of *P-h* curves and scratch tests. The porous titanium substrate only influenced the type and size of the gelatin porosity, thus indirectly influencing the tribo-mechanical behavior. Fig. 6 shows the micro-mechanical loading-unloading curves of the coated c.p. Ti porous substrates, comparing the pore sizes for non-crosslinked and crosslinked gelatin. On the other hand, Fig. 7 displays the *P-h* curves comparing the non-crosslinked and crosslinked gelatin for the same pore sizes (100–200 and 355–500 µm). Just smaller and larger pores were compared to evaluate the effect of the porosity. The characteristic parameters are summarized in Table 2. For the same type of coating, the penetration depth (maximum and permanent) increases with the pore size, independently of the gelatin (non-crosslinked or crosslinked). However, the elastic recovery is higher in the case of the non-crosslinked gelatin. For the same size of the pores, the characteristic parameters, penetration depth and elastic recovery, were similar for the two tested coatings.

The trends observed in Figs. 6 and 7 allowed the following observations. On the one hand, regardless of the type of gelatin (with and without crosslinking), as gelatin was less dense and/or presented larger

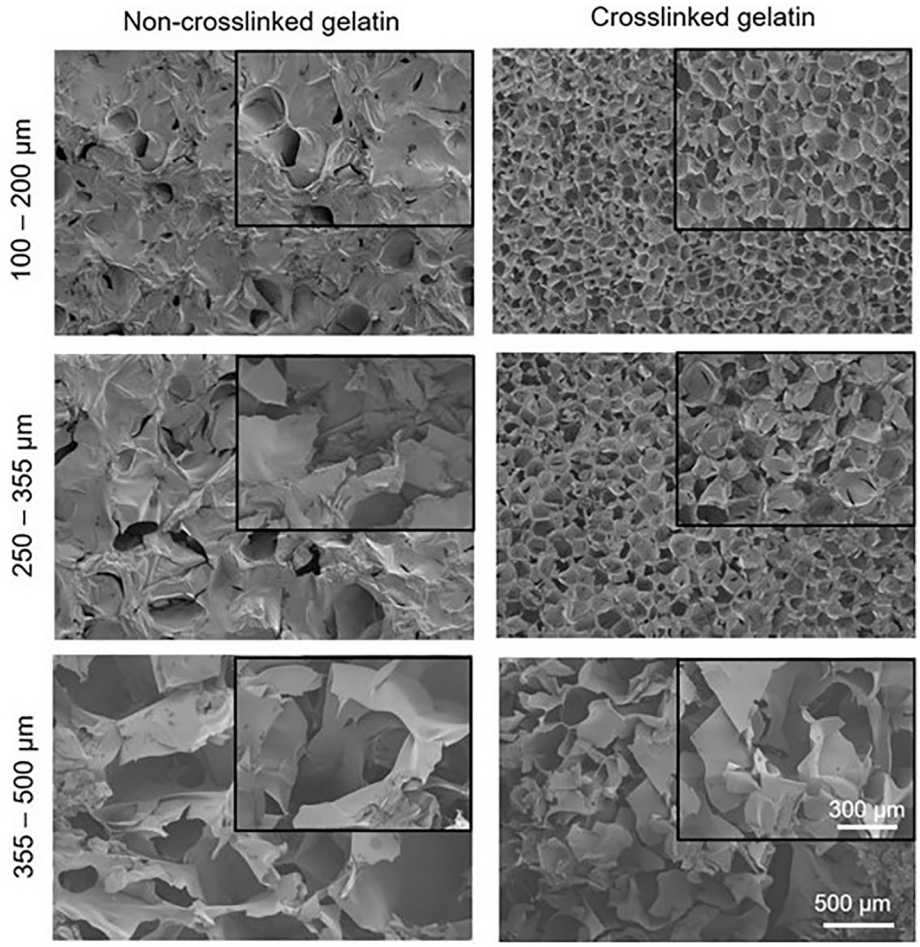

Fig. 4. SEM top-view micrographs of the bioactive gelatin coatings. Common scale bar. Inset: higher magnification images.

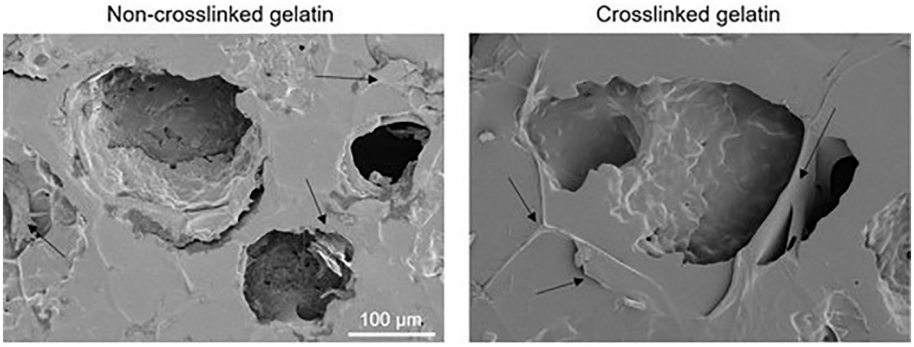

Fig. 5. SEM top-view micrographs of the surface of 100–200 µm porous Ti substrate after removing the gelatin coating. Arrows indicate the rest of gelatin covering the flat areas and inside the pores. Common scale bar.

pores, and its microhardness decreased (permanent penetration depth increased). On the other hand, an inverse relationship was generally observed between the pore size of gelatin (Fig. 3) and the elastic recovery in relative terms. This fact was less representative in gelatins with the presence of crosslinking (the "shape memory" effect prevailed regarding the type of pores).

A more detailed analysis of Fig. 7a, allowed to indicate a particular behavior, since up to 0.6 N of applied load, the crosslinked gelatin presented "softer" behavior, while for higher loads the trend was reversed. This behavior of the crosslinked gelatin obtained on the c.p. Ti substrate with pores in a size range of 100–200 µm could be related to the role of the channels in the honeycomb-like structure. So, for small loads only the influence of an independent channel would be evaluated while (see Fig. 7a, load lower than 0.6 N), as the deformation increases, the contribution of the rest of the contiguous channels would be relevant and, therefore, the crossovers would play an important role. A similar analysis over the gelatin obtained on substrates with a larger spacer size (355–500 µm) revealed the inverse trend (Fig. 7b). In this case, there is no honeycomb structure, so the behavior was more isotropic (there was not preferential direction) and the crosslinks were responsible for the greater stiffness observed in this type of gelatin. It is worth to note that although a homogenization of the behavior was observed for 1 N, the relative elastic recovery of the crosslinked gelatin was much higher, corroborating their role in the micromechanical behavior of this type of

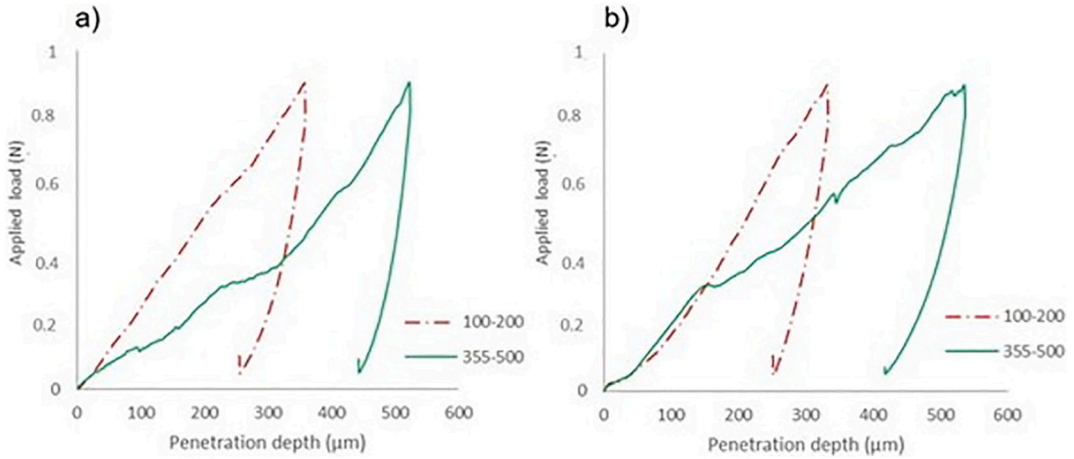

Fig. 6. *P-h* curves of porous c.p. Ti coated with a) non-crosslinked and b) crosslinked gelatin.

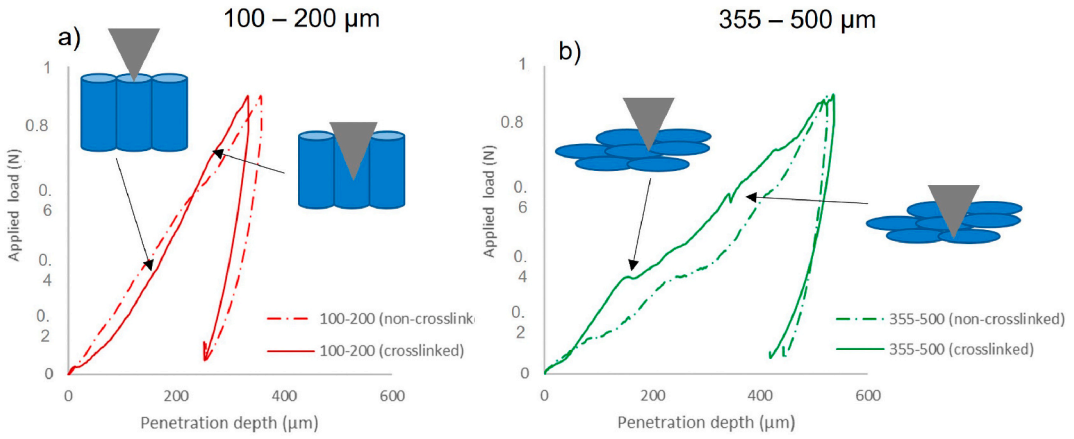

Fig. 7. *P-h* curves of porous c.p. Ti of range pore sizes of a) 100–200 and b) 355–500 μm.

Table 2
Characteristic parameters of *P-h* curves.

Spacer size range (μm)		Non-crosslinked gelatin		Crosslinked gelatin	
		100–200	355–500	100–200	355–500
Penetration depth (μm)	Maximum value	359	524	334	537
	Permanent value	248	440	249	411
Elastic recovery	Absolut value (μm)	111	84	85	126
	Relative value (%)	31	16	25	23

material. In this curve, like-steps were observed. They could be related to the morphology and stacking of the gelatin and their effects over the load during the breakage process of the gelatin layers (see the arrows in Fig. 7b, indicating the drop of the load).

Concerning the scratch test, the main parameters are summarized in Table 2 and the curves are displayed in Figs. 8 and 9, in which the influence of the pore size range and the gelatin type (non-crosslinked or crosslinked) are shown. The elastic relaxation behavior was evaluated by the differences between the *in-situ* penetration (plastic and elastic deformation) and the real plastic deformation (penetration depth) associated to the scratch tests is shown in Fig. 8, for the smaller and larger pore sizes of the tested coated samples, while Fig. 9 displays the graphic corresponding to the plastic deformation comparing the samples by the type of gelatin (non-crosslinked and crosslinked) and by the size of the pores (100–200 and 355–500 μm). Table 3 summarizes the absolute elastic recovery of the studied samples. In the case of the crosslinked gelatin coating, all pore sizes presented similar values of the absolute elastic recovery, which were lower than the non-crosslinked gelatin. However, in the case of the non-crosslinked gelatin, there was a clear difference of the measured values, being higher for the larger pore sizes.

A general analysis of the scratch results revealed an arch shape, which suggested that the gelatins were not homogeneous over the whole surface of the disc, being denser at the edge (note that the scratch resistance was higher, that is, the penetration was lower). This fact could be produced by an edge effect during the gelatin manufacturing process. In the same sense, the resistance to scratching in the central area was lower, which indicates that the gelatin was softer in this area (greater porosity or larger pores). In this context, crosslinked gelatins and/or deposited on porous c.p. Ti substrates with the smallest range of porous sizes, presented a greater homogeneity.

In view of these results, it could be concluded that, on the one hand, for the same type of gelatin, the elastic recovery was inversely proportional to the interconnected porosity of the gelatin (see Fig. 2) since smaller range pores size of the substrates presented higher P_i of the gelatin, therefore, the elastic recovery was lower (for example, for the 100–200 μm substrate and non-crosslinked gelatin, $P_i = 43.4\%$ and the relative elastic recovery was 23% *versus* the 13% observed for the 355–500 μm substrate coated by crosslinked gelatin with a $P_i = 38.4\%$. On the other hand, the penetration depth was directly proportional to P_i.

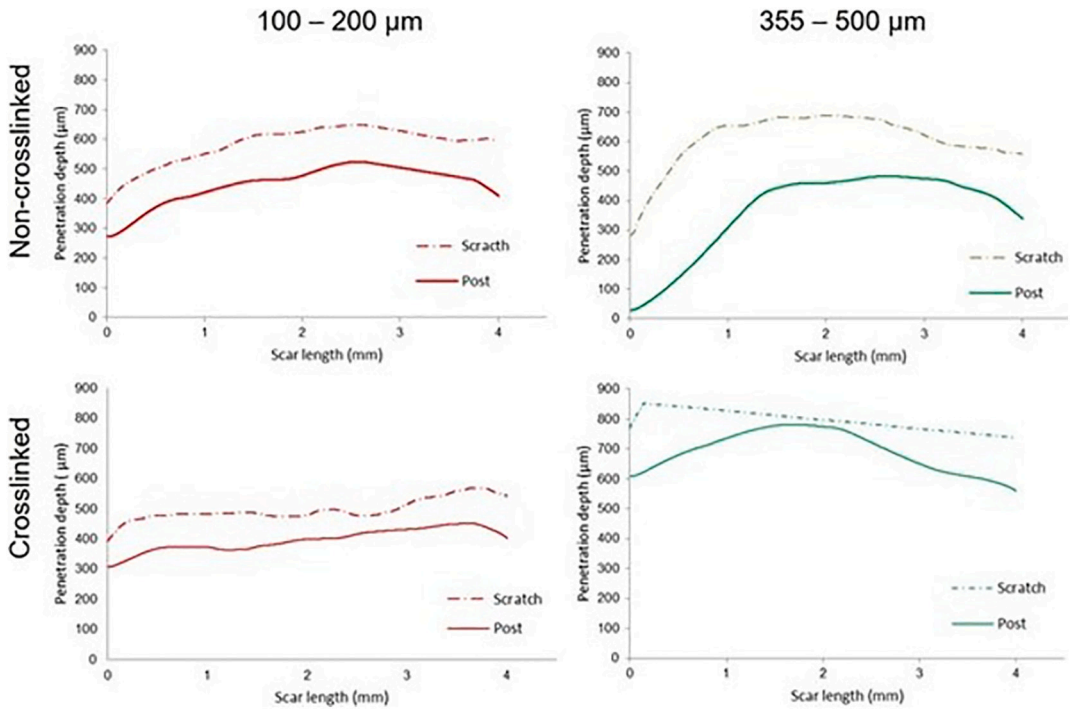

Fig. 8. Penetration depth during and after the scratch tests.

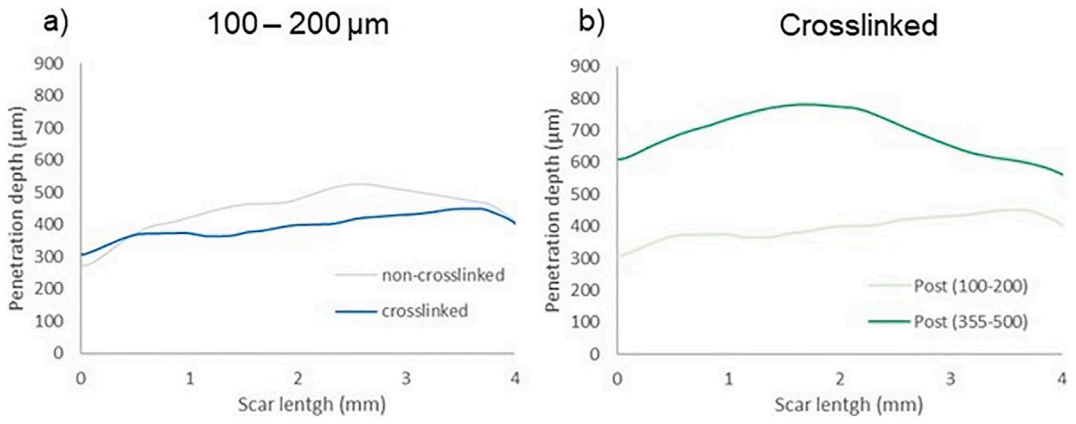

Fig. 9. Permanent plastic deformation after the scratch, comparing a) non-crosslinked *vs* crosslinked gelatin for the smaller pore size range substrates and b) the pore size range for the crosslinked gelatin.

Table 3
Absolute and relative permanent plastic deformation values.

	Size of the pores (µm)	Non-crosslinked gelatin		Crosslinked gelatin	
		100–200	355–500	100–200	355–500
Permanent deformation depth	Maximum (µm)	525	489	450	782
	Average (µm)	449 ± 63	368 ± 57	396 ± 36	692 ± 40
Elastic recovery	Absolut (µm)	135 ± 13	241 ± 87	100 ± 21	103 ± 58
	Relative (%)	23 ± 4	42 ± 20	20 ± 4	13 ± 7

Note: It is important to remark that the gelatin behavior observed in *P-h* curves and scratch tests could be different since *P-h* curves are static tests while scrath tests are considered to be dynamic. Besides, it is worth to emphasize the role of the crosslinking and the porosity (morhology, percentage, size and interconnectivity) on the analyzed behavior.

Besides, for the same type of substrate, the elastic recovery of gelatin decreased in the case of the crosslinked gelatin.

Finally, although *in vitro* and *in vivo* studies will be planned as future work to demonstrate the applicability of this approach to treat osteochondral defects, the biocompatibility of gelatin is widely known. In fact, Hernandez et al. [48] proved that the use of gelatin is not only biocompatible but also enables greater fibroblast attachment. In another example, Sun et al. [49] verified that gelatin-based composites were not cytotoxic *in vitro*, using a NIH 3 T3 murine cell line, and *in vivo*, in 12-week-old male Wistar rats. Also, the non-thrombogenicity of gelatin-based hydrogels has been confirmed by Krüger-Genge et al. [50].

4. Conclusions

In this work, c.p. Ti porous substrates were fabricated by the spacer-holder techniques with three different pore size ranges (100–200 µm, 250–355 µm and 355–500 µm) and coated with two types of gelatinous materials, one as a linear polymer (non-crosslinked) and another one

crosslinked. The role of the crosslink, as well as the morphology, size and degree of interconnectivity of the porosity of the gelatin samples on their tribo-mechanical behavior were analyzed. These coated substrates were evaluated with the aim of finding an improved biomechanical and biofunctional behavior. Concerning the biomechanical behavior, the intermediate size (250–355 μm) represented the equilibrium in terms of mechanical properties. Besides, it presented a suitable size for bone ingrowth. The biofunctional behavior was also evaluated in terms of the infiltration and adherence of the two types of gelatins. In general, both were able to adhere independently of the substrate. Lower microhardness (larger permanent penetration depth) and lower elastic recovery were observed for higher porosity gelatins (non-crosslinked and crosslinked). These preliminary results open a new promising route to manufacture composite porous implants which are potential candidates to develop alternative treatments, not only for osteochondral defects, but also for other kind of damages in which tissues of different nature need to be perfectly joined.

CRediT authorship contribution statement

Y. Torres: Conceptualization, Writing – review & editing, Supervision, Project administration, Funding acquisition. **B. Begines:** Methodology, Investigation, Writing – original draft, Writing – review & editing. **A.M. Beltrán:** Methodology, Investigation, Writing – original draft, Writing – review & editing. **A.R. Boccaccini:** Conceptualization, Writing – review & editing.

Declaration of competing interest

The authors declare that they have no known competing financial interests.

Acknowledgments

The authors dedicate this paper to the memory of Juan J. Pavón Palacio (University of Antioquia, Colombia). Also, thanks to the students L. Aranda and A. Cuéllar, as well as the laboratory technician, J. Pinto, for the support in characterization of the samples. This work was supported by the Ministry of Science and Innovation of Spain under the grant PID2019-109371GB-I00.

References

[1] S. Harada, G.A. Rodan, Control of osteoblast function and regulation of bone mass, Nature. 423 (2003) 349–355, https://doi.org/10.1038/nature01660.
[2] G.A. Rodan, T.J. Martin, Therapeutic approaches to bone diseases 289 (2000) 1508–1514, https://doi.org/10.1126/science.289.5484.1508.
[3] O. Demontiero, C. Vidal, G. Duque, Aging and bone loss: new insights for the clinician, Ther. Adv. Musculoskelet. Dis. 4 (2012) 61–76, https://doi.org/10.1177/1759720X11430858.
[4] Q. Li, J.C. yiu Cheng, Q. Jiang, W.Y. wai Lee, Role of sirtuins in bone biology: potential implications for novel therapeutic strategies for osteoporosis, Aging Cell (2021) 1–21, https://doi.org/10.1111/acel.13301.
[5] R.D. Crowninshield, A.G. Rosenberg, S.M. Sporer, Changing demographics of patients with total joint replacement, Clin. Orthop. Relat. Res. (2006) 266–272, https://doi.org/10.1097/01.blo.0000188066.01833.4f.
[6] W.H. Organization, Musculoskeletal conditions, (2021). https://www.who.int/news-room/fact-sheets/detail/musculoskeletal-conditions (accessed May 7, 2021).
[7] J. Yang, Y.S. Zhang, K. Yue, A. Khademhosseini, Cell-laden hydrogels for osteochondral and cartilage tissue engineering, Acta Biomater. 57 (2017) 1–25, https://doi.org/10.1016/j.actbio.2017.01.036.
[8] X. Duan, X. Zhu, X. Dong, J. Yang, F. Huang, S. Cen, F. Leung, H. Fan, Z. Xiang, Repair of large osteochondral defects in a beagle model with a novel type i collagen/glycosaminoglycan-porous titanium biphasic scaffold, Mater. Sci. Eng. C. 33 (2013) 3951–3957, https://doi.org/10.1016/j.msec.2013.05.040.
[9] J.F. Mano, R.L. Reis, Osteochondral defects: present situation and tissue engineering approaches, J. Tissue Eng. Regen. Med. 1 (2007) 261–273, https://doi.org/10.1002/term.37.
[10] D. Schaefer, I. Martin, P. Shastri, R.F. Padera, R. Langer, L.E. Freed, G. Vunjak-Novakovic, *In vitro* generation of osteochondral composites, Biomaterials 21 (2000) 2599–2606, https://doi.org/10.1016/s0142-9612(00)00127-7.
[11] W. Swieszkowski, B.H.S. Tuan, K.J. Kurzydlowski, D.W. Hutmacher, Repair and regeneration of osteochondral defects in the articular joints, Biomol. Eng. 24 (2007) 489–495, https://doi.org/10.1016/j.bioeng.2007.07.014.
[12] P. Nooeaid, J.A. Roether, E. Weber, D.W. Schubert, A.R. Boccaccini, Technologies for multilayered scaffolds suitable for interface tissue engineering, Adv. Eng. Mater. 16 (2014) 319–327, https://doi.org/10.1002/adem.201300072.
[13] J. Gaviria, A. Alcudia, B. Begines, A.M. Beltrán, J. Villarraga, R. Moriche, J. A. Rodríguez-Ortiz, Y. Torres, Synthesis and deposition of silver nanoparticles on porous titanium substrates for biomedical applications, Surf. Coat. Technol. 406 (2021), 126667, https://doi.org/10.1016/j.surfcoat.2020.126667.
[14] A. Civantos, A.M. Beltrán, C. Domínguez-Trujillo, M.D. Garvi, J. Lebrato, J. A. Rodríguez-Ortiz, F. García-Moreno, J.V. Cauich-Rodriguez, J.J. Guzman, Y. Torres, Balancing porosity and mechanical properties of titanium samples to favor cellular growth against bacteria, Metals (Basel) 9 (2019) 1039, https://doi.org/10.3390/met9101039.
[15] Y. Yang, N. Oh, Y. Liu, W. Chen, S. Oh, M. Appleford, S. Kim, K. Kim, S. Park, J. Bumgardner, W. Haggard, J.L. Ong, Enhancing osseointegration using surface-modified titanium implants, JOM. 58 (2006) 71–76, https://doi.org/10.1007/s11837-006-0146-1.
[16] K.H. Frosch, A. Drengk, P. Krause, V. Viereck, N. Miosge, C. Werner, D. Schild, E. K. Stürmer, K.M. Stürmer, Stem cell-coated titanium implants for the partial joint resurfacing of the knee, Biomaterials. 27 (2006) 2542–2549, https://doi.org/10.1016/j.biomaterials.2005.11.034.
[17] A.M. Beltrán, B. Begines, A. Alcudia, J.A. Rodríguez-Ortiz, Y. Torres, Biofunctional and tribomechanical behavior of porous titanium substrates coated with a bioactive glass bilayer (45S5-1393), ACS Appl. Mater. Interf. 12 (2020), https://doi.org/10.1021/acsami.0c07318.
[18] X.Y. Zhang, G. Fang, S. Leeflang, A.A. Zadpoor, J. Zhou, Topological design, permeability and mechanical behavior of additively manufactured functionally graded porous metallic biomaterials, Acta Biomater. 84 (2019) 437–452, https://doi.org/10.1016/j.actbio.2018.12.013.
[19] H.J. Yun, D. Abolhasani, T.W. Hwang, T. Lee, J.H. Kim, Y.H. Moon, Fabrication of porous titanium parts by powder bed fusion of Ti-TiH2blended powder, J. Mater. Res. Technol. 9 (2020) 3026–3037, https://doi.org/10.1016/j.jmrt.2020.01.033.
[20] R. Kobatake, K. Doi, T. Kubo, Y. Makihara, Y. Oki, M. Yokoi, H. Umehara, K. Tsuga, Novel fabrication of porous titanium by a resin-impregnated titanium substitution technique for bone reconstruction, RSC Adv. 9 (2019) 1625–1631, https://doi.org/10.1039/c8ra08744j.
[21] C. Chen, Y. Hao, X. Bai, J. Ni, S.M. Chung, F. Liu, I.S. Lee, 3D printed porous Ti6Al4V cage: effects of additive angle on surface properties and biocompatibility; bone ingrowth in beagle tibia model, Mater. Des. 175 (2019), 107824, https://doi.org/10.1016/j.matdes.2019.107824.
[22] A.M. Beltrán, A. Alcudia, B. Begines, J.A. Rodríguez-Ortiz, Y. Torres, Porous titanium substrates coated with a bilayer of bioactive glasses, J. Non-Cryst. Solids 544 (2020), https://doi.org/10.1016/j.jnoncrysol.2020.120206.
[23] R. Moriche, A.M. Beltrán, B. Begines, J.A. Rodríguez-Ortiz, A. Alcudia, Y. Torres, Influence of the porosity and type of bioglass on the micro-mechanical and bioactive behavior of coated porous titanium substrates, J. Non-Cryst. Solids 551 (2021), https://doi.org/10.1016/j.jnoncrysol.2020.120436.
[24] Y. Torres, J.A. Rodríguez, S Arias, M Echeverry, S Robledo, V Amigo, J.J. Pavón, Processing, characterization and biological testing of porous titanium obtained by space-holder technique, J. Mater. Sci. 47 (2012) 6565–6576, https://doi.org/10.1007/s10853-012-6586-9.
[25] D.P. Mondal, M. Patel, S. Das, A.K. Jha, H. Jain, G. Gupta, S.B. Arya, Titanium foam with coarser cell size and wide range of porosity using different types of evaporative space holders through powder metallurgy route, Mater. Des. 63 (2014) 89–99, https://doi.org/10.1016/j.matdes.2014.05.054.
[26] J. Jia, A.R. Siddiq, A.R. Kennedy, Porous titanium manufactured by a novel powder tapping method using spherical salt bead space holders: characterization and mechanical properties, J. Mech. Behav. Biomed. Mater. 48 (2015) 229–240, https://doi.org/10.1016/j.jmbbm.2015.04.018.
[27] M. Rahimi, G. Charmi, K. Matyjaszewski, X. Banquy, J. Pietrasik, Recent developments in natural and synthetic polymeric drug delivery systems used for the treatment of osteoarthritis, Acta Biomater. 114 (2020) 31–52, https://doi.org/10.1016/j.actbio.2020.12.005.
[28] Z. Wang, L. Han, T. Sun, J. Ma, S. Sun, L. Ma, B. Wu, Extracellular matrix derived from allogenic decellularized bone marrow mesenchymal stem cell sheets for the reconstruction of osteochondral defects in rabbits, Acta Biomater. 118 (2020) 54–68, https://doi.org/10.1016/j.actbio.2020.10.022.
[29] S. Critchley, E.J. Sheehy, G. Cunniffe, P. Diaz-Payno, S.F. Carroll, O. Jeon, E. Alsberg, P.A.J. Brama, D.J. Kelly, 3D printing of fibre-reinforced cartilaginous templates for the regeneration of osteochondral defects, Acta Biomater. 113 (2020) 130–143, https://doi.org/10.1016/j.actbio.2020.05.040.
[30] A. Smandri, A. Nordin, N.M. Hwei, K.Y. Chin, I. Abd Aziz, M.B. Fauzi, Natural 3D-printed bioinks for skin regeneration and wound healing: a systematic review, Polymers (Basel). 12 (2020), https://doi.org/10.3390/polym12081782.
[31] A. Gaspar-Pintiliescu, A.M. Stanciuc, O. Craciunescu, Natural composite dressings based on collagen, gelatin and plant bioactive compounds for wound healing: a review, Int. J. Biol. Macromol. 138 (2019) 854–865, https://doi.org/10.1016/j.ijbiomac.2019.07.155.
[32] A. Francesko, P. Petkova, T. Tzanov, Hydrogel dressings for advanced wound management, Curr. Med. Chem. 25 (2019) 5782–5797, https://doi.org/10.2174/0929867324666170920161246.
[33] Y. Xu, Z. Wang, Y. Hua, X. Zhu, Y. Wang, L. Duan, L. Zhu, G. Jiang, H. Xia, Y. She, G. Zhou, Photocrosslinked natural hydrogel composed of hyaluronic acid and

gelatin enhances cartilage regeneration of decellularized trachea matrix, Mater. Sci. Eng. C 120 (2021), 111628, https://doi.org/10.1016/j.msec.2020.111628.
[34] K. Ngadimin, A. Stokes, P. Gentile, A.M. Ferreira-Duarte, Biomimetic hydrogels designed for cartilage tissue engineering, Biomater. Sci. i (2021), https://doi.org/10.1039/d0bm01852j.
[35] L. Li, F. Yu, L. Zheng, R. Wang, W. Yan, Z. Wang, J. Xu, J. Wu, D. Shi, L. Zhu, X. Wang, Q. Jiang, Natural hydrogels for cartilage regeneration: modification, preparation and application, J. Orthop. Transl. 17 (2019) 26–41, https://doi.org/10.1016/j.jot.2018.09.003.
[36] B. Tissue, A bibliometric analysis of the global trend of using alginate, 2021, pp. 1–17.
[37] S. Ranganathan, K. Balagangadharan, N. Selvamurugan, Chitosan and gelatin-based electrospun fibers for bone tissue engineering, Int. J. Biol. Macromol. 133 (2019) 354–364, https://doi.org/10.1016/j.ijbiomac.2019.04.115.
[38] Z. Dong, Q. Yuan, K. Huang, W. Xu, G. Liu, Z. Gu, Gelatin methacryloyl (GelMA)-based biomaterials for bone regeneration, RSC Adv. 9 (2019) 17737–17744, https://doi.org/10.1039/c9ra02695a.
[39] ASTM F67-13, Standard specification for unalloyed titanium, in: For Surgical Implant Applications (UNS R50250, UNS R50400, UNS R50550, UNS R50700), ASTM Int., West, Conshohocken, PA, 2017 (2017).
[40] Y. Torres, P. Trueba, J. Pavón, I. Montealegre, J.A. Rodríguez-Ortiz, Designing, processing and characterization of titanium cylinders with graded porosity: an alternative to stress-shielding solutions, Mater. Des. 63 (2014) 316–324, https://doi.org/10.1016/j.matdes.2014.06.012.
[41] ASTM C373-14, Standard Test Method for Water Absorption, Bulk Density, Apparent Porosity, and Apparent Specific Gravity of Fired Whiteware Products, Ceramic Tiles, and Glass Tiles, ASTM Int., West, Conshohocken, PA, 2014, https://doi.org/10.1520/C0373-14, 2014.
[42] P. Trueba, A.M. Beltrán, J.M.J.M. Bayo, J.A. Rodríguez-Ortiz, D.F. Larios, E. Alonso, D.C. Dunand, Y. Torres, A.M. Beltran, J.M.J.M. Bayo, J.A. Rodriguez-Ortiz, D.F. Larios, E. Alonso, D.C. Dunand, Y. Torres, Porous titanium cylinders obtained by the freeze-casting technique: influence of process parameters on porosity and mechanical behavior, Metals (Basel). 10 (2020) 188, https://doi.org/10.3390/met10020188.
[43] H. Liang, Y. Yang, D. Xie, L. Li, N. Mao, C. Wang, Z. Tian, Q. Jiang, L. Shen, Trabecular-like Ti-6Al-4 V scaffolds for orthopedic: fabrication by selective laser melting and *in vitro* biocompatibility, J. Mater. Sci. Technol. 35 (2019) 1284–1297, https://doi.org/10.1016/j.jmst.2019.01.012.
[44] C. Domínguez-Trujillo, A.M. Beltrán, M.D. Garvi, A. Salazar-Moya, J. Lebrato, D. J. Hickey, J.A. Rodríguez-Ortiz, P.H. Kamm, C. Lebrato, F. García-Moreno, T. J. Webster, Y. Torres, Bacterial behavior on coated porous titanium substrates for biomedical applications, Surf. Coat. Technol. 357 (2019) 896–902, https://doi.org/10.1016/j.surfcoat.2018.10.098.
[45] C. Domínguez-Trujillo, F. Ternero, J.A. Rodríguez-Ortiz, J.J. Pavón, I. Montealegre-Meléndez, C. Arévalo, F. García-Moreno, Y. Torres, Improvement of the balance between a reduced stress shielding and bone ingrowth by bioactive coatings onto porous titanium substrates, Surf. Coat. Technol. 338 (2018) 32–37, https://doi.org/10.1016/j.surfcoat.2018.01.019.
[46] A. Rodriguez-Contreras, M. Punset, J.A. Calero, F.J. Gil, E. Ruperez, J.M. Manero, Powder metallurgy with space holder for porous titanium implants: a review, J. Mater. Sci. Technol. 76 (2021) 129–149, https://doi.org/10.1016/j.jmst.2020.11.005.
[47] S. Matsuda, H. Iwata, N. Se, Y. Ikada, Bioadhesion of gelatin films crosslinked with glutaraldehyde, J. Biomed. Mater. Res. 45 (1999) 20–27, https://doi.org/10.1002/(SICI)1097-4636(199904)45:1<20::AID-JBM3>3.0.CO;2-6.
[48] J.L. Hernandez, J. Park, S. Yao, A.K. Blakney, H.V. Nguyen, B.H. Katz, J.T. Jensen, K.A. Woodrow, Effect of tissue microenvironment on fibrous capsule formation to biomaterial-coated implants, Biomaterials. 273 (2021), 120806, https://doi.org/10.1016/j.biomaterials.2021.120806.
[49] C.K. Sun, C.J. Ke, Y.W. Lin, F.H. Lin, T.H. Tsai, J.S. Sun, Transglutaminase cross-linked gelatin-alginate-antibacterial hydrogel as the drug delivery-coatings for implant-related infections, Polymers (Basel). 13 (2021) 1–14, https://doi.org/10.3390/polym13030414.
[50] A. Krüger-Genge, C. Tondera, S. Hauser, S. Braune, J. Görs, T. Roch, R. Klopfleisch, A.T. Neffe, A. Lendlein, J. Pietzsch, F. Jung, Immunocompatibility and non-thrombogenicity of gelatin-based hydrogels, Clin. Hemorheol. Microcirc. 77 (2021) 335–350, https://doi.org/10.3233/CH-201028.